Transient Phase-Induced Nucleation in Ionic Liquid Crystals and Size-Frustrated Thickening

Liangbin Li,* Jan Groenewold, and Stephen J. Picken

Polymer Materials and Engineering, Delft University of Technology, Julianalaan 136, 2628 BL Delft, and Dutch Polymer Institute, P.O. Box 902, 5600 AX Eindhoven, The Netherlands

Received July 22, 2004. Revised Manuscript Received October 21, 2004

The crystallization behavior of amphiphilic ionic imidazolium liquid crystals has been studied with in situ small- and wide-angle X-ray scattering. We found that below the melting point four crystal phases exist. Their relative stability is checked by investigating the mutual transitions and using a heating scan. The following sequence is observed: triclinic extended bilayer > triclinic double bilayer > perpendicular double bilayer. A transient phase with a low density, which may not be stable at any temperature, is observed to serve as the nucleation mechanism for all three phases. The large size of the transient crystals is found to frustrate the layer thickening, which occurs from the double bilayer to extended bilayer transition. The competition between the thermodynamic driving force and the imposed constraints leads to the formation of wrinkles. The influence of water on the crystallization behavior is demonstrated to be indirect, which reduces the size of the crystals.

Introduction

Upon cooling materials from the melt, during crystal nucleation a transient phase can occur that converts to the stable form during the later stages of growth.[1−8] Not only are such transient phases intermediate states on route to the final structure, but they also can be a key to the understanding of crystallization. The occurrence of a transient phase not only can change the crystallization process, but may also result in various different final structures and morphologies. However, transient states are intrinsically difficult to observe, and their study has been limited. In contrast to normal long-lived metastable states, there is no temperature at which the transient phase will remain present indefinitely. To investigate the transient states, computer simulation[6,7] and time-resolved techniques, such as synchrotron radiation, are employed. For instance, with time-resolved synchrotron X-ray scattering, a transient metastable rotator phase is observed during the crystallization of hexadecane.[8]

1-Alkyl-3-methylimidazolium salts are examples of room-temperature ionic liquids, which have some excellent properties that make them suitable for many applications such as as green solvents and for batteries and fuel cells.[9−13] Upon increasing the alkyl tail up to 12 carbons, a smectic liquid crystal (or lamellar) phase can be obtained.[14,15] There is considerable interest in the structural features of ionic liquid crystals, for example, as oriented solvents or reactants, as templates for the synthesis of mesoporous and zeolitic materials, and in the formation of ordered thin films (see ref 16 and references therein). By analogy to the simple *n*-alkanes, ionic liquid crystals can be a model system to study crystallization from an oriented liquid.[8,17−20] Crystallization from a smectic liquid crystal state with prealigned molecules certainly has the required nucleation rate, while the imidazolium headgroup may slow the transition from a metastable to a stable state. Studies on this model system are expected to shed light on the phase behavior of lipids[21,22] and the ongoing debate about preordering during polymer crystallization.[23−26]

It was reported that liquid crystal 1-alkyl-3-methylimidazolium salts can crystallize into two different structures with a layer spacing ratio of about 2.[14−16,27,28] Both structures have

* To whom correspondence should be addressed. Present address: Unilever Research & Development Vlaardingen, Olivier van Noortlaan 120, 3133 AT Vlaardingen, The Netherlands. E-mail: liangbin.li@unilever.com.

(1) Ostwalds, W. *Z. Phys. Chem.* **1897**, *22*, 286.
(2) Sutton, M.; et al. *Phys. Rev. Lett.* **1989**, *62*, 288−291.
(3) Hikosaka, M.; et al. *J. Macromol. Sci.* **1992**, *B31*, 87−131.
(4) Keller, A.; Cheng, S. Z. D. *Polymer* **1998**, *39*, 4461−4487.
(5) Sirato, E. B.; Herhold, A. B.; Varma-Nair, M. *J. Chem. Phys.* **2000**, *113*, 8225−8236.
(6) Ten Wolde, P. R.; Ruiz-Montero, M. J.; Frenkel, D. *Phys. Rev. Lett.* **1995**, *75*, 2714−2717.
(7) Shen, Y. C.; Oxtoby, D. W. *Phys. Rev. Lett.* **1996**, *77*, 3585−3588.
(8) Sirota, E. B.; Herhold, A. B. *Science* **1999**, *283*, 529−532.
(9) Welton, T. *Chem. Rev.* **1999**, *99*, 2071−2084.
(10) Welton, T., Ed. *Ionic liquid in synthesis*; Wiley-VCH Verlag: Weinheim, Germany, 2003.
(11) Xu, W.; Angell, C. A. *Science* **2003**, *302*, 422−425.
(12) Rogers, R. D.; Seddon, K. R. *Science* **2003**, *302*, 792−793.
(13) Brennecke, J. F.; Maginn, E. J. *AIChE J.* **2001**, *47*, 2384−2389.
(14) Gordon, C. M.; Holbrey, J. D.; Kennedy, A. R.; Seddon, K. R. *J. Mater. Chem.* **1998**, *8*, 2627−2636.
(15) Bowlas, C. J.; Bruce, D. W.; Seddon, K. R. *Chem. Commun.* **1996**, 1625−1626.
(16) Bradley, A. E.; Hardacre, C.; Holbrey, J. D.; Johnston, S.; Macmath, S. E.; Nieuwenhuyzen, M. *Chem. Mater.* **2002**, *14*, 629−635.
(17) Kraack, H.; Deutsch, M.; Sirota, E. B. *Macromolecules* **2000**, *33*, 6174.
(18) Sirato, E. B.; Single, D. M. *J. Chem. Phys.* **1994**, *101*, 10873−10881.
(19) Herhold, A. B.; King, H. E., Jr.; Sirato, E. B. *J. Chem. Phys.* **2002**, *116*, 9036−9050.
(20) Ungar, G. *Polymer* **1993**, *34*, 2050.
(21) Sato, K. *Chem. Eng. Sci.* **2001**, *56*, 2255−2265.
(22) Small, D. M. *The Physical Chemistry of Lipids*; Plenum Press: New York, 1986.
(23) See for a recent review, see: Heeley, E. L.; et al. *Faraday Discuss.* **2002**, *122*, 343−361.
(24) Li, L. B.; de Jeu, W. H. *Macromolecules* **2003**, *36*, 4862−4867.
(25) Li, L. B.; de jeu, W. H. *Phys. Rev. Lett.* **2004**, *92*, 075506.
(26) Ungar, G.; Zheng, X. B. *Chem. Rev.* **2001**, *101*, 4157−4188.

10.1021/cm048811f CCC: $30.25
Published on Web 12/15/2004

a triclinic unit cell. The different layer spacings were explained on the basis of structures comprising either a double bilayer with interdigitated alkyl chains or an extended bilayer in which the alkyl chains are packed end-to-end. This was attributed to hydrogen bonding bridged by water molecules between adjacent layers.[28] However, direct evidence for this especially during the formation process is still absent. It is worth noting that the observation of different characteristic layer spacings is quite general in lipids and other amphiphilic molecules. Skin lipids (ceramides) crystallize in structures with layer spacings of about 6 and 13 nm,[29,30] which result in different skin barriers. The understanding of the origin of the different layer spacings of 1-alkyl-3-methylimidazolium salts can be extended to other amphiphilic molecules, which show similar structural features.[22]

In this work, we apply time-resolved X-ray scattering to study the crystallization process of hexadecyl-3-methylimidazolium chloride ([C_{16}-mim]Cl) and octadecyl-3-methylimidazolium chloride ([C_{18}-mim]Cl). Transient phases are observed during nucleation to the final stable state. The presence of water and frustration are found to be the major factors for the formation of the different layer spacings. Contrary to the idea of hydrogen bonding bridged by water, the presence of water favors the formation of larger layer spacings rather than preventing layer thickening.

Experimental Section

Materials. The [C_{16}-mim]Cl and [C_{18}-mim]Cl materials (ca. 100%) were purchased from Acros and used after being dried in a vacuum at 70 °C for 24 h. Materials with different water concentrations were obtained by exposing the samples to normal air for different periods of time. The resulting water concentration was measured by thermogravitometric analysis (TGA). The simplified phase diagram is about K 66 Sm-A 222 I for [C_{16}-mim]Cl and K 72 Sm-A 222 I for [C_{18}-mim]Cl.[14−16,27,28] In fact, as we show in this work, four different crystal modifications can occur below the melting point.

Characterization. Simultaneous WAXS and SAXS measurements were made using an in-house setup with a rotating anode X-ray generator (Rigaku RU-300H, 18 kW) equipped with two parabolic multilayer mirrors (Bruker, Karsruhe), giving a highly parallel beam of monochromatic Cu Kα radiation ($\lambda = 0.154$ nm) with a divergence of about 0.012°. The X-ray flux of this arrangement is an order of magnitude larger than for conventional pinhole collimation in combination with a nickel filter. The beam size was defined by two sets of slit pinholes, while a guard slit pinhole was placed in front of the sample to cut parasitic scattering from the beam-defining slits and the mirrors. The SAXS intensity was collected with a two-dimensional (2-D) gas-filled wire detector (Bruker Hi-star). A semitransparent beamstop in front of the area detector allowed us to monitor the intensity of the direct beam. The WAXS intensity was recorded by a linear position-sensitive detector (PSD-50M, M. Braun, Germany), which could be rotated around the beam path to measure in either the meridional or the equatorial direction. The SAXS and WAXS intensities were normalized to the intensity of the direct beam attenuated by the semitransparent beamstop and plotted vs q, where $q = 4\pi(\sin\theta)/\lambda$ and 2θ is the scattering angle. A Linkam CSS450 temperature-controlled shear system was employed as the sample stage. Samples were tightly sealed in a nylon washer with Kapton windows. During the experiments, the samples were first heated to the smectic phase at 80 °C and then cooled to the predetermined temperatures for isothermal crystallization. Specific experimental procedures were applied on some samples, which are described in the Results. Because the phase behaviors of [C_{16}-mim]Cl and [C_{18}-mim]Cl are rather similar, in many cases we only present the results from one of them.

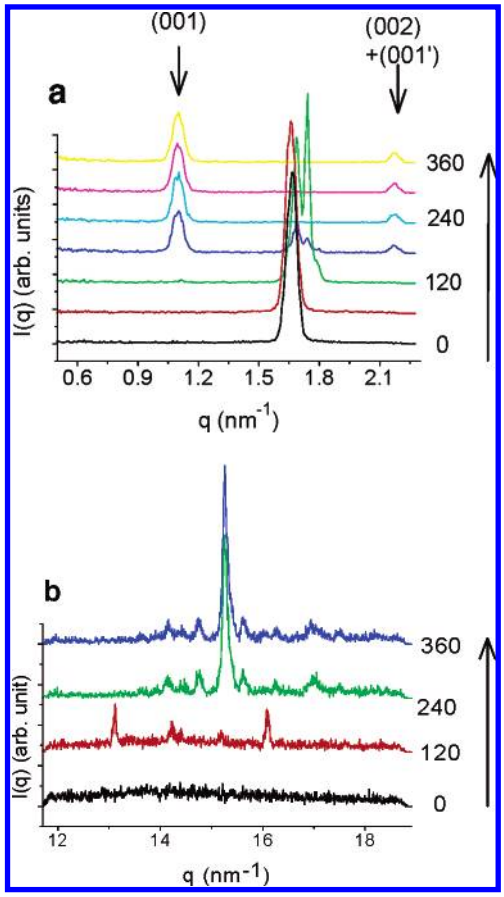

Figure 1. (a) Integrated one-dimensional SAXS patterns and (b) corresponding WAXS patterns of the [C_{16}-mim]Cl sample (1.9 wt % water) during isothermal crystallization at 52 °C. The numbers in the figure indicate the crystallization time in seconds.

Results

Figure 1a shows a series of representative integrated one-dimensional SAXS curves (from 2-D patterns) of [C_{16}-mim]-Cl during isothermal crystallization at 52 °C. This specific choice of temperature was found to be the optimum for observing the transient phase. The corresponding one-dimensional WAXS patterns are displayed in Figure 1b. The crystallization starts from an ordered smectic phase, which has a scattering peak corresponding to a periodicity of 3.78 nm at 52 °C. About 120 s after the crystallization temperature is reached, crystals with a periodicity of 3.64 nm appear, which give rise to sharp scattering points in the SAXS patterns. This transient phase also shows peaks in the WAXS

(27) De Roche, J.; Gordon, C. M.; Imrie, C. T.; Ingram, M. D.; Kennedy, A. R.; Lo Celso, F.; Triolo, A. *Chem. Mater.* **2003**, *15*, 3089−3097.
(28) Downard, A.; Earle, M. J.; Hardacre, C.; Macmath, S. E. J.; Nieuwenhuyzen, M.; Teat, S. J. *Chem. Mater.* **2004**, *16*, 43−48.
(29) Bouwstra, J. A.; Gooris, G. S.; Cheng, K.; Weerheim, A.; Bras, W.; Ponec, M. *J. Lipid Res.* **1996**, *37*, 999−1011.
(30) Bouwstra, J. A.; Gooris, G. S.; Dubbelaar, F. E. R.; Ponec, M. *J. Lipid Res.* **2001**, *42*, 1759−1770.

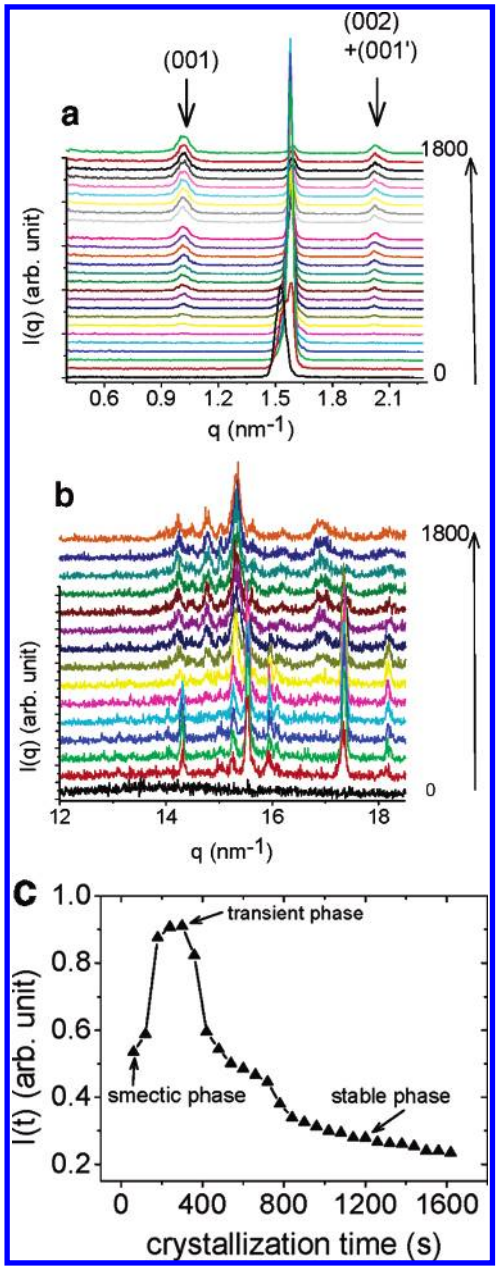

Figure 2. (a) Integrated one-dimensional SAXS patterns and (b) corresponding WAXS patterns of [C_{18}-mim]Cl sample (1.8 wt % water) during isothermal crystallization at 60 °C. The numbers in the figure indicate the crystallization time in seconds. (c) Integrated SAXS intensity vs crystallization time.

patterns (see Figure 1b). Upon increasing the crystallization time, this transient phase transforms into a different crystal state. These stable crystals have a larger layer periodicity of 5.72 nm and a completely different set of WAXS reflection peaks, which have triclinic symmetry and are denoted as triclinic extended bilayers. We designate the transient phase as rotator double bilayers on the basis of their layer spacing and similarity to *n*-alkanes and nonadecylcyclohexane.[5,8]

The SAXS and WAXS patterns of [C_{18}-mim]Cl during a crystallization process at 60 °C are displayed in parts a and b, respectively, of Figure 2. Similar to that of [C_{16}-mim]Cl, the crystallization starts with a layer spacing (3.97 nm) slightly smaller than that of the original smectic phase (4.10 nm), while the structure with larger spacing (6.20 nm) develops after the initial formation of the transient phase. The transition from the metastable transient phase is also demonstrated by the appearance and disappearance of its WAXS peaks (see Figure 2b). The integrated SAXS intensity gives further evidence of the transition of smectic liquid crystal−transient metastable crystal−stable crystal (see Figure 2c), which increases for the transient phase and decreases for the final stable crystals. This process nicely coincides with the peak positions of the three phases in SAXS patterns (Figure 2a). The SAXS patterns in both Figures 1a and 2a show scattering peaks at the (002) position, which have much higher intensity than that of a normal higher order peak. Evidently, these scattering peaks are composed of a (001′) peak from crystals with a double bilayer structure and the (002) peak from the extended bilayer crystals. This is also confirmed by the peak width as it is found that the (002) peak is much sharper than (001). The transient phases of both ionic salts are also observed at other temperatures (small supercooling) and during a nonisothermal crystallization with a small cooling rate.

During the crystallization process, large size transient crystals are formed, as indicated by the very sharp scattering peaks (instead of a homogeneous ring) in the 2-D SAXS patterns.[31] The nucleation of the final triclinic bilayers first occurs from these large crystals, while the large crystals can also persist and do not transform to the extended bilayers. Figure 3a shows a 2-D SAXS pattern of a crystallized [C_{18}-mim]Cl sample, which reveals the coexistence of the triclinic and double bilayers where the large size of the crystals frustrates the required thickening. A strong off-speckle scattering (streaks in the *q* direction) accompanies the sharp scattering peaks, which leads to a significant contribution to the tail of the peak without influencing the width. Figure 3c shows the integrated one-dimensional SAXS pattern of these peaks. The integrated azimuthal angle range is illustrated in Figure 3b by the fan sector. To obtain a single orientation scattering, the isotropic scattering pattern is employed as the background profile. A good fitting is achieved with a Lorentzian function rather than with a Gaussian function (solid and dashed−dotted lines in Figure 3c, respectively), while the peak is sharp and gives a correlation length on the order of 100 nm. Line shape analysis[32−35] gives a value of −1.65 for the asymptotic slope for the extended bilayer, while −2.6 is found for the double bilayer (see Figure 3d).

The influence of water on the crystallization behavior is presented in Figure 4 showing SAXS patterns of [C_{16}-mim]-Cl obtained during crystallization at 53 °C at various water concentrations. With a water concentration of 1.9 wt %, the same transition process at 52 °C is observed (Figure 4a). A higher water concentration leads to a faster transition process (Figure 4b), while a lower water concentration completely

(31) The real time SAXS patterns (powerpoint movie) of [C_{18}-mim]Cl during the crystallization process at 60 °C. See the Supporting Information.
(32) de Jeu, W. H.; Ostrovskii, B. I.; Shalaginov, A. N. *Rev. Mod. Phys.* **2003**, *75*, 181−235.
(33) Caillie, A. *C. R. Acad. Sci. Paris* **1972**, *B274*, 891−893.
(34) Kaganer, V. M.; Ostrovsky, B. I.; de Jeu, W. H. *Phys. Rev. A* **1991**, *44*, 8158−8166.
(35) Wong, G. C. L.; de Jeu, W. H.; Shao, H.; Liang, K. S.; Zentel, R. *Nature* **1997**, *389*, 576−579.

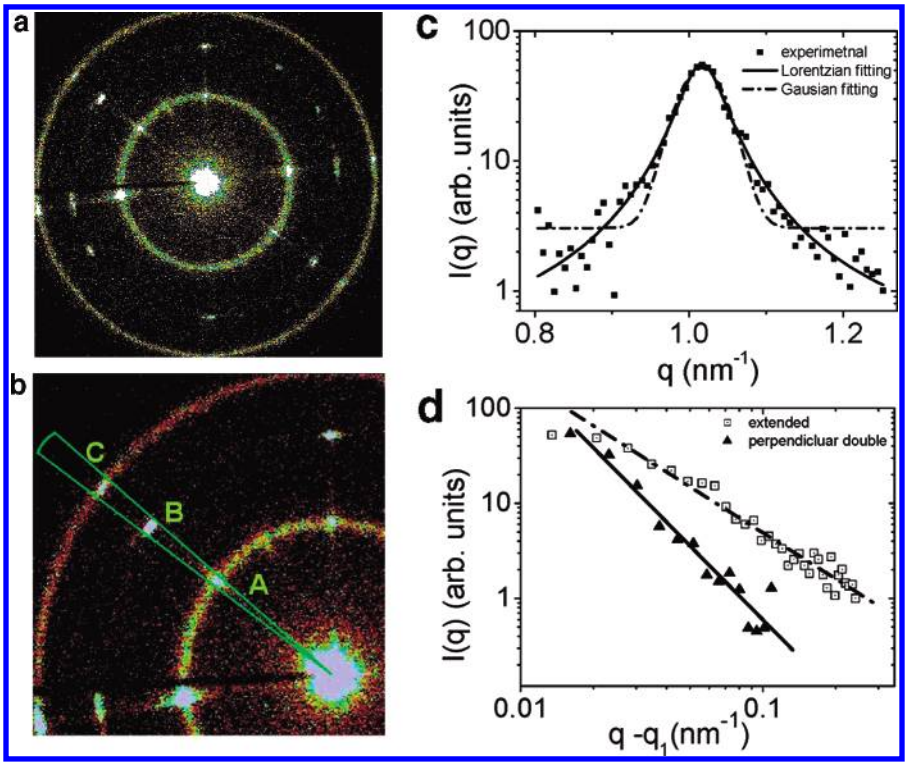

Figure 3. (a) Two-dimensional SAXS pattern of a [C_{18}-mim]Cl sample after isothermal crystallization at 60 °C. (b) A quarter from (a) illustrating the integrating azimuthal angle range, where points A−C denote the scattering points from the triclinic extended bilayer and perpendicular and triclinic double bilayers, respectively. (c) Integrated one-dimensional scattering pattern at point A in (b) within the azimuthal angle range indicated in (b). (d) Double logarithmic plot of intensity I vs $q - q_1$ of peaks at points A and B in (b).

suppresses the transition to triclinic crystals with a larger or smaller spacing (Figure 4c). Alternatively, here the final state has a slightly smaller layering (3.54 nm) than that of the transient state (3.69 nm). The corresponding WAXS patterns of Figure 4c are shown in Figure 4d. Several small diffraction peaks appear at the beginning of crystallization and disappear after the transition; this is further confirmation of the presence of the transient phase. We cannot deduce the formed crystal structure on the basis of limited scattering peaks. Nevertheless, the layer spacing of 3.54 nm suggests that it is an orthorhombic or monoclinic double bilayer structure with interdigitated alkyl chains (nearly) perpendicular to the layer surface. For convenience, we denote this phase as perpendicular double bilayers.

In our experiments, it is rather difficult to obtain the triclinic double bilayer structure with interdigitated alkyl chains. Figure 5A displays a SAXS pattern of a [C_{16}-mim]-Cl sample by a fast quenching from 80 °C. The sample has a low water concentration, as it was dried at 80 °C in a vacuum for 48 h. In this case, triclinic and perpendicular double bilayers are formed, which give scattering peaks at q of about 2.25 and 1.77 nm^{-1}, respectively. Following a slow cooling, only the latter is obtained. Another sample was dried at 40 °C in a vacuum for one week and contains 1.3 wt % water. Because this temperature is far below the melting point, the original crystal size is expected to be preserved. Figure 5B shows the SAXS pattern of the crystallized sample following a slow cooling with a rate of 1 °C/min from 80 °C. At the end only the triclinic extended bilayer structure is formed.

The thermodynamic stability is further studied by a heating scan. Figure 6a shows SAXS patterns of a crystallized [C_{18}-mim]Cl sample initially with triclinic extended bilayers alone at different temperatures during a heating scan, while SAXS patterns of the [C_{16}-mim]Cl sample originally containing triclinic double bilayers are displayed in Figure 6b. During these processes, the samples keep their initial morphology and structure till melting into the smectic phase. The SAXS and WAXS patterns of a crystallized [C_{16}-mim]Cl with only the perpendicular double bilayers during a step heating process are given in parts c and d, respectively, of Figure 6. The X-ray scattering patterns reveal that a transition from the perpendicular double bilayers to the triclinic extended bilayers occurs at a temperature around 55 °C. This transition does not occur if we start from a sample with triclinic bilayers (see Figure 6a,b).

Discussion

The above experimental results show the phase behavior of these ionic liquid salts is far more complicated than just a simple crystal to smectic transition. Four crystal phases are observed: triclinic extended, triclinic double, perpendicular double, and transient rotator double bilayers. In fact, different sets of WAXS peaks were observed from the transient phases, which suggests the rotator double bilayers can have different packings. This is hardly a surprise because *n*-alkanes are known to have five rotator phases.[18]

The four phases show different thermodynamic stabilities as revealed by X-ray scattering obtained during the heating scans. The triclinic extended bilayer structure is the most stable phase, which has a melting point of about 65 °C for [C_{16}-mim]Cl. The second most stable phase is the double bilayer structure with a melting point of about 62 °C. The perpendicular double bilayer transforms to the triclinic

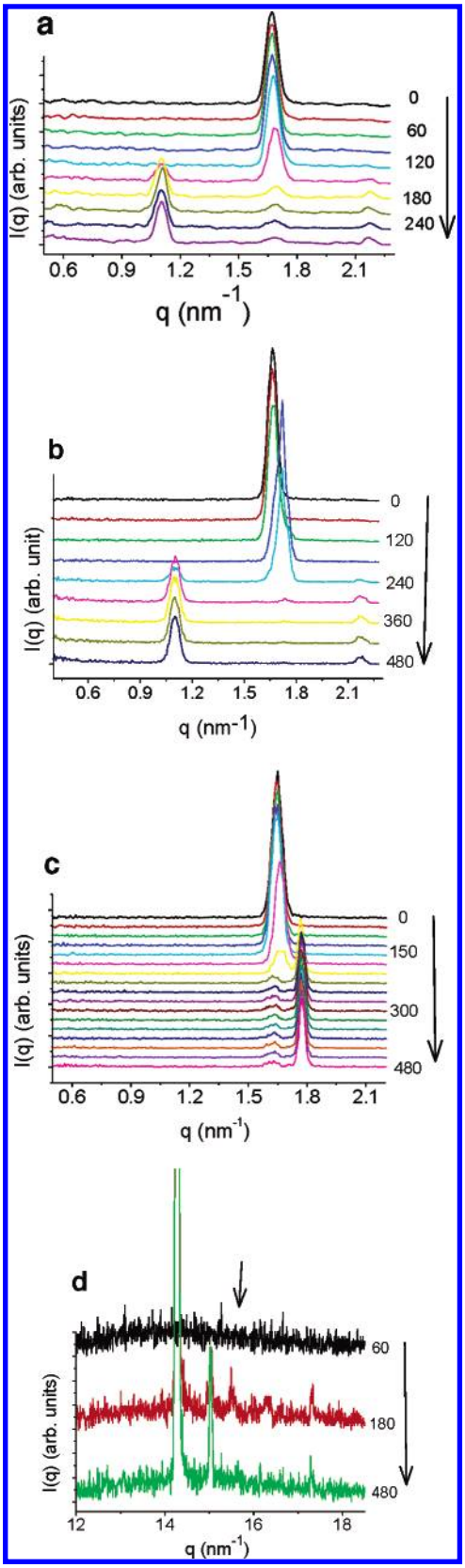

Figure 4. SAXS patterns of [C_{16}-mim]Cl samples with different water concentrations during isothermal crystallization at 53 °C: (a) 2.9 wt %, (b) 1.9 wt %, (c) 1.6 wt %. (d) Corresponding WAXS patterns of sample (c). The numbers in the figure indicate the crystallization time in seconds.

extended structure at a temperature of about 55 °C, which is the least stable phase. Finally, there is the transient phase, which appears at slight supercooling and which may be thermodynamically unstable at any temperature.

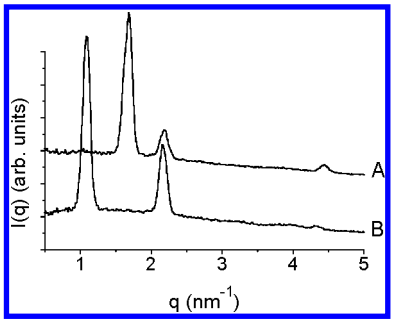

Figure 5. SAXS patterns of [C_{16}-mim]Cl samples obtained through (A) (0.5 wt % water) quenching and (B) (1.3 wt % water) slow cooling (1 °C/min) from 80 °C.

Evidently, the transient phase has a high molecular mobility, and similar structures of the rotator phases of *n*-alkanes are expected. This is indeed supported by the observation of only a few diffraction peaks in WAXS (see Figure 1b). In general, *n*-alkanes with similar molecular lengths (C_{16} and C_{18}) have two rotator phases, R_I and R_{II}, which show orthorhombic and hexagonal symmetry, respectively.[18] In these two rotator phases the alkyl chains are perpendicular to the layer surface. The layer spacing of the transient phase is slightly smaller than that of the smectic phase. This suggests the alkyl chains in the smectic phase are somewhat overstretched and the transient phase may have a lower packing density of alkyl chains than that of the smectic phase. The overstretching seems plausible if we consider the abnormally high isotropization temperature (T_{iso} = 222 °C). The crystallization temperature is far below this point. Following the idea of microphase separation in a block copolymer, the alkyl chains are stretched further with increasing supercooling, $\Delta T = T_{iso} - T_K$, where T_K is the crystallization temperature.[36] Similarly, in our materials the large smectic temperature range may result in the overstretching of the short alkyl chains. The low packing density of the transient phase can be checked by measuring the scattering intensity. Comparing the scattering intensities from the smectic, transient, and final stable crystal phases, we find that the transient phase gives the highest scattering intensities (see Figure 2c). The imidazolium and chloride ions are located at the interface of the smectic layers, which yields a higher density than that of the alkyl chains (see Figure 7).[14−16,27,28] During the smectic liquid crystal−crystal transition, the packing density of imidazolium and chloride ions is not expected to vary significantly. Thus, the increase of the scattering intensity reveals the decrease of the density in the alkyl layers, because the scattering intensity is proportional to $\Delta\rho^2$, where $\Delta\rho$ is the density difference between the layer center and interface.[37] This implies that the alkyl layers in the transient phase have a density lower than that of the smectic phase. This is in line with the rotator I phase (R_I) in pure *n*-alkanes as well as for alcohols and olefin derivatives, which show a negative linear compressibility.[38]

(36) Hamley, I. W. *The Physics of Block Copolymers*; Oxford University Press: New York, 2000.
(37) Lindner, P., Zemb, Th., Eds. *Neutrons, x-rays and light: scattering methods applied to soft condensed matter*; Elsevier: Amsterdam, 2002.
(38) Sirota, E. B.; King, H. E., Jr. *Science* **1998**, *281*, 143.

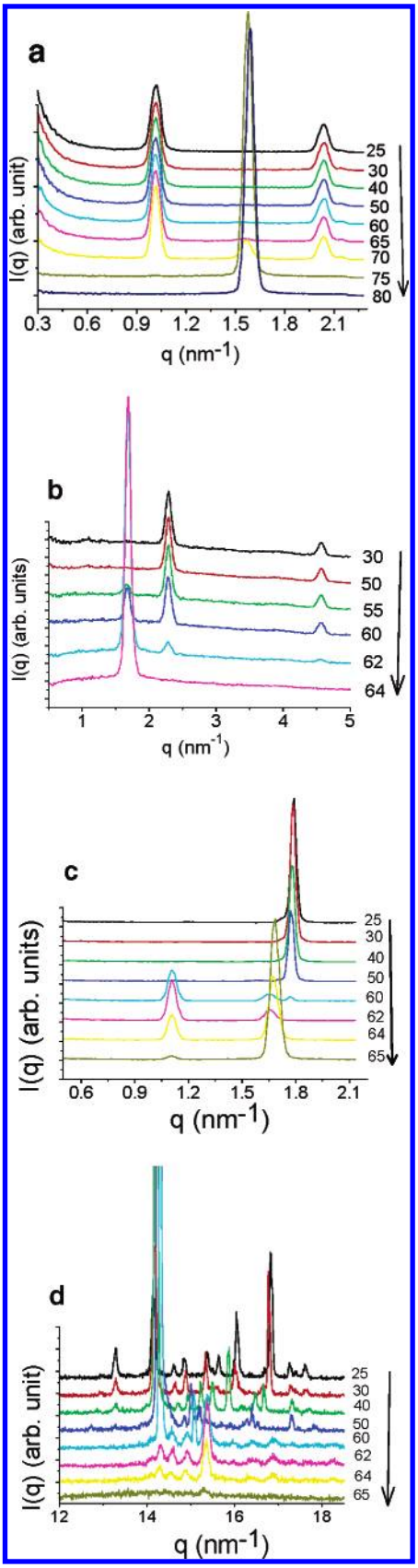

Figure 6. SAXS patterns of amphiphilic salt crystals obtained during a heating scan: (a) [C_{18}-mim]Cl with only the triclinic extended bilayer, (b) [C_{16}-mim]Cl with only the triclinic double bilayer, and (c) with only the perpendicular double bilayer. The numbers in the figure indicate the temperature (°C).

The relative stability and transformations among these phases are schematically shown in Figure 7. Upon cooling of the ionic liquid crystals to the crystallization temperature, the highly stretched alkyl chains easily adopt a crystal structure with a high mobility, which is similar to the behavior of the rotator phases of *n*-alkanes and nonadecylcyclohexane. This transient phase has a short lifetime. The transient phase has three possible destinations—the triclinic extended bilayer, perpendicular double bilayer, and triclinic double bilayer. The metastability and chain mobility of the transient phase are expected to promote the nucleation and growth of three phases. However, only the former two are usually obtained, while a fast cooling is required for the formation of the triclinic double bilayers. This suggests that the transient phase may not be the necessary pathway to the formation of triclinic double bilayers. At the same crystallization temperature, the thermodynamic driving force to the extended bilayer is higher than that of the double bilayer on the basis of its higher melting temperature. After nucleation through the transient phase, a fast crystallization rate of the extended bilayer is achieved due to the low nucleation barrier. This consequently reduces the chance for growing the triclinic double bilayers. In addition to the competition from the extended bilayer, the perpendicular double bilayer is another competitor. This phase has the advantage of a faster kinetic pathway because the layer spacing is similar to that of the transient phase. Having to compete with these two phases, it is certainly difficult for the triclinic double bilayer to catch the opportunity for growth. Only if the extended bilayer is frustrated significantly by the large size of the crystal (this will be discussed later) does the triclinic double bilayer have a chance to grow (see Figures 2 and 3). During a heating scan, the perpendicular double bilayer transforms into the triclinic extended one; no transformations are observed between the triclinic double and the perpendicular double bilayers or the triclinic double and extended bilayers.

The crystallization starts from an ordered melt, with a specific molecular orientation and layer spacing, which assists subsequent crystallization. Kinetically, during the formation of a crystal with a layer spacing comparable to that of the smectic precursor, the molecules only need to perform local conformational adjustment rather than a large-scale motion. The sharp scattering points in the SAXS patterns indicate a fast formation of large metastable crystals.[31] The transition to the stable phase begins in these large crystals, as the azimuthal angle position of both phases is at the same place (see Figure 3). These large crystals are also the last regions to transform into the stable triclinic extended bilayers.[31] In some cases the large crystals transform into the perpendicular double bilayer structure rather than the triclinic extended one. The ultimate destination is controlled by the size of the transient crystals. The layer spacing of the triclinic extended bilayer is about 1.6 times that of the transient phase. Therefore, a significant expansion along the layer normal has to take place. When the crystals are small and randomly oriented, as in the situation of the normal powder diffraction, the pressure against this expansion is relatively small. In this case, the thermodynamic driving force is enough to overcome the resistance and the triclinic double bilayer is obtained (see Figures 1, 4a,b, and 5). Increasing the crystal size, the distance that the molecules

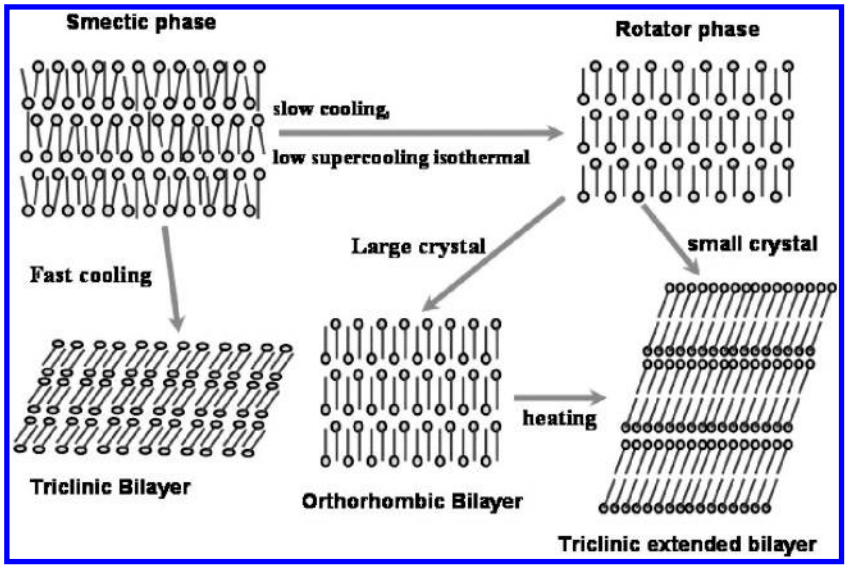

Figure 7. Scheme describing the relative stability and mutual transitions of the smectic phase and the four crystal phases.

have to diffuse becomes too large and the pressure starts to inhibit the transition from occurring. Instead, the alternative structure—the perpendicular double layer—is formed. We call this effect size frustration.

The choice of either the triclinic extended or the perpendicular double bilayer is certainly not a simple yes or no situation. The triclinic extended bilayer is thermodynamically stable, which always drives the molecules toward this state. We believe there is another alternative mechanism to avoid the pressure against thickening or thinning. As discussed above, a negative pressure in the lateral sides of the bilayers is created during the transition from the transient phase to the triclinic extended bilayer, while the layer normal direction creates a positive pressure. This picture is somewhat similar to the phenomenon of wrinkling. Compression of a rigid fiber embedded in a soft matrix generally leads to a wrinkled structure.[39] By analogy, wrinkles are expected to form during the layer thickening (see Figure 8). The two-dimensional scattering pattern and the peak fitting and line shape analysis on the one-dimensional curves support the formation of wrinkles (see Figure 3). In the q or 2θ direction, strong streaks are observed around the scattering points. Compared to that of the scattering at points B and C in Figure 3b, the width of the peak at point A is much wider, which indicates a smaller correlation length. This small correlation length could originate from a wide distribution of layer spacings and a frequent change of the layer orientation. It is a characteristic feature of wrinkles to periodically change the layer orientation, which consequently reduces the effective correlation length. In fact, the occurrence of wrinkles in large crystals has been reported before by Nazaki et al.[40] in large crystals of *n*-alkane.

Using a scattering instrument with synthetic multilayer mirrors for the X-ray optics, it would normally not be possible to distinguish a Gaussian peak from a Lorentzian peak, due to limited instrument resolution. The unambiguous discrimination of the scattering peak shape at point A (Figure 3b) suggests the amplitude of the wrinkles is rather large.[32−35] The peak fitting and line shape analysis surprisingly show that the large crystal size frustration mechanism results in the extended bilayer structure forming a state more like a liquid crystal glass (mesoglass) rather than a true crystal.[32−35,41] In smectic layers, the thermal fluctuation destroys translational order,[42] which leads the structure factor S in the direction perpendicular to the layers to have an asymptotic power-law form:

$$S(0,0,q_z) \approx \frac{1}{|q_z - q_m|^{2-\eta_m}} \qquad (1)$$

where q_z represents the wave vector along the density wave and q_m is the position of the mth order of diffraction. The exponent η_m is given by

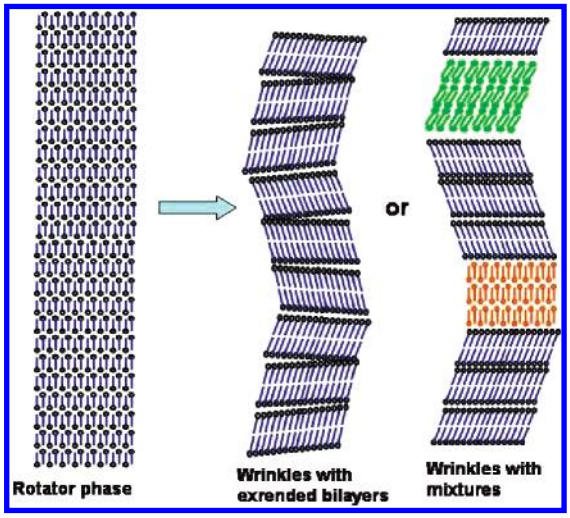

Figure 8. Scheme showing the formation of wrinkles due to the large crystal size of the transient phase. The real wavelength of the wrinkles will contain many more layers, as indicated from the rather small correlation length.

(39) Groenewold, J. *Physica A* **2001**, *298*, 32−45.
(40) Nozaki, K.; Hikosaka, M. *J. Mater. Sci.* **2000**, *35*, 1239−1252.
(41) Jéröme, B.; Commandeur, J. *Nature* **1997**, *386*, 589−591.
(42) Landau, L. D. In *Collected paper of L. D. Landau*; ter Haar, Ed.; Gordon & Breach: New York, 1965; pp 193−216.

$$\eta_m = q_m^2 k_B T/(8\pi(BK)^{1/2} \quad (2)$$

which is directly related to the elastic constants of the smectic structure: K is the bending modulus and B is the layer compression modulus (T is temperature, and k_B is Boltzmann's constant). Following Caille's calculation,[33] a plot of log S vs $q - q_1$ for the smectic layers gives a slope with a limit at -2 (see Figure 3d) due to the Landau−Peierls instability,[42] while a crystal with long-range order can give a value smaller than -2.[32−35] Because the isotropic scattering part was already subtracted in Figure 3d, the scattering curve is more or less like the situation for single-crystal diffraction. Both scattering peaks at B and C in Figure 3b give slopes smaller than -2, whereas the peak at A, scattered by the extended bilayers, has a slope of -1.65. Here, the long-range order is destroyed by external compression rather than by thermal fluctuations as in the case of a smectic layers. Then k_BT in eq 2 should be replaced by a compression (elastic) energy. Taking into account the confinement by the environment, crystals with wrinkles may even represent a thermodynamically stable state. However, the coupling between the elastic properties and the environment is more complicated during a dynamical development process,[39] and the competition from other phases can complicate matters further. For example, in Figure 8 inserting a double bilayer structure may assist in the switching of the orientation, as it may reduce the required energy for bending. This picture is supported by the X-ray scattering results. The double bilayer structure is found to have the same orientation as the triclinic extended structure, as evidenced by the sharp scattering points in the SAXS patterns (see Figure 3).

The idea that molecular water bridges prevent the triclinic double layers from thickening is not consistent with our observation.[16] Following a fast quenching, the triclinic double bilayer structure can be obtained in the sample containing a low water content, as determined by TGA (see Figure 5). Moreover, the presence of water promotes the formation of extended bilayers rather than double bilayers (see Figure 4). Thus, the presence of water does not have a direct correlation to the formation of triclinic double bilayers. Without the influence of water, the perpendicular double bilayer dominates in crystallization. The presence of water apparently promotes the bilayer thickening. The question is as follows: How do water molecules enhance the mobility? In all the crystalline phases, the water molecules will avoid the region of the alkyl chains. Assisted by hydrogen-bonding or hydrophilic interactions, it is likely that the water resides preferentially at the interface of the bilayers. However, as suggested by Downard et al.[28] the hydrogen bond bridges between adjacent layers suppress the thickening. During the heating scan, the initial perpendicular bilayer transforms into the triclinic extended one with a higher stability (see Figure 6c,d). This suggests that the presence of water changes the kinetic pathway rather than the thermodynamic force. Therefore, the effect of water on the thickening is indirect. On the basis of the above idea of size-frustrated thickening, the role of water on the crystallization of these ionic salts can be understood. The water does nothing but reduce the size of the crystals. This in fact is common knowledge both for edible kitchen salt and for other inorganic salts. After the sample is dried at temperatures below the melting point, the crystal size is preserved. Via this effect, a low water content can still allow the thickening of the bilayers (see Figure 5B).

Conclusions

With in situ small- and wide-angle X-ray scattering, the thermal stability and the crystallization behavior of [C_{16}-mim]-Cl and [C_{18}-mim]Cl have been investigated. Four crystal phases were observed in these amphiphilic ionic salts, each with a different thermal stability. The low-density transient phase, which may not be stable at any temperature, shows high molecular mobility and serves as a nucleus for the formation of the other three crystal structures. The most stable phase is the triclinic double bilayer, with a melting point of 65 °C for [C_{16}-mim]Cl, which can be obtained through direct crystallization from the smectic phase or by transformation from the perpendicular double bilayer structure at a temperature of about 55 °C during heating. The triclinic double bilayer is the second most stable one, which melts directly at a temperature around 62 °C. The large crystal size of the transient phase prohibits the thickening from the double bilayer to the extended bilayer structure. Wrinkles form as the compromise between the kinetic pathway and the thermodynamic driving force. The presence of water tends to reduce the crystal size, which in turn affects the subsequent crystallization. Our results demonstrate that amphiphilic ionic salts not only have potential for various applications but also can serve as an interesting model system for fundamental studies on nucleation. The effect of water and the size frustration mechanism may be shared by other amphiphilic lipids such as ceramides and fatty acids.[21,22,29,30]

Acknowledgment. We thank Wim H. de Jeu (AMOLF, Amsterdam) for helpful discussions and providing the opportunity to use the SAXS/WAXS setup and Ben Norder (Delft) for TGA measurements. This work forms part of the research program of the Dutch Polymer Institute.

Supporting Information Available: Two-dimensional SAXS patterns of [C_{18}-mim]Cl during crystallization at 60 °C (ZIP). This material is available free of charge via Internet at http://pubs.acs.org.

CM048811F